Experimental Section

Synthesis of Zn nanosheets

All chemicals were used as received without further purification. Zn nanosheets were fabricated by an electrochemical reduction method[1]. Typically, 0.03 M urea and 0.002 M $ZnCl_2$ were dissolved in 50 mL deionized water followed by adjusting the solution pH to 5. The obtained solution was transferred into a Teflon-lined stainless-steel autoclave and kept at 100 °C for 24 h. After cooling, the precipitates were collected and washed with deionized water/ethanol and then drying under vacuum. The dried precipitates were further calcined at 450 °C for 1 h under air atmosphere. The obtained ZnO nanosheets were then electrochemically reduced to Zn nanosheets at -0.75 V (vs RHE) in Ar-bubbled 0.5 M $NaHCO_3$ solution.

Electrochemical experiments

Electrochemical performance was investigated with a standard three-electrode system at a CHI-760E electrochemical workstation with as-prepared catalyst coated on a carbon cloth (CC), a graphite rod and an Ag/AgCl (saturated KCl) as the working, the counter and the reference electrodes, respectively. All potentials were referenced to the reversible hydrogen electrode (RHE) by following equation: E_{RHE} (V)=$E_{Ag/AgCl}$+0.198+0.059×pH. The NORR tests were performed using an H-type two-compartment electrochemical cell separated by a Nafion 211 membrane. Prior to NORR test, all feeding gases were purified through two glass bubblers containing 4 M KOH solution and the cathodic compartment was purged with Ar for at least 30 min to remove residual oxygen[2]. During the potentiostatic testing, NO flow (99.9%, 20 mL min^{-1}) was continuously fed to the cathodic compartment. After electrolysis for 1 h at various potentials, liquid and gas products were detected by colorimetry and gas chromatography (GC, Shimadzu GC2010), respectively. The detailed procedures were provided in our previous publications[3]**.** NH_3 yield rate and NH_3-Faradaic efficiency (FE_{NH3}) were calculated by the following equation[4]:

$$NH_3 \text{ yield} = (c \times V) / (17 \times t \times A) \quad (1)$$

$$FE_{NH3} = (5 \times F \times c \times V) / (17 \times Q) \times 100\% \quad (2)$$

where c (μg mL^{-1}) is the measured NH_3 concentration, V (mL) is the volume of electrolyte in the cathode chamber, t (s) is the electrolysis time and A is the surface area of CC (1×1 cm^2), F (96500 C mol^{-1}) is the Faraday constant, Q (C) is the total quantity of applied electricity.

Characterizations

Transmission electron microscopy (TEM) and high-resolution transmission electron microscopy (HRTEM) were recorded on a Tecnai G^2 F20 microscope. X-ray diffraction (XRD) pattern was collected on a Rigaku D/max 2400 diffractometer. X-ray photoelectron spectroscopy (XPS) analysis was conducted on a PHI 5702 spectrometer. The UV-vis absorbance measurements were performed on a MAPADA P5 spectrophotometer.

Calculation details

Spin-polarized density functional theory (DFT) calculations were carried out on a Cambridge sequential total energy package (CASTEP)[5]. The exchange-correlation interactions were treated within the generalized gradient approximation (GGA) in the form of the Perdew-Burke-Ernzerhof (PBE) functional. To ensure all atoms were fully relaxed for each system, the convergence tolerance was set as 1.0×10^{-5} eV for energy and 0.02 eV $Å^{-1}$ for force. A Gamma-point centered 3×3×1 k-mesh was adopted for structural optimizations, and a plane wave cutoff was set to 400 eV. Zn (101) was modeled by a 4×4 supercell, and a vacuum space of around 15 Å was set along the z direction to avoid the interaction between periodical images.

The free energies (ΔG, 298 K) for each reaction were given after correction[6]:

$$\Delta G = \Delta E + \Delta ZPE - T\Delta S \tag{3}$$

where ΔE is the adsorption energy, ΔZPE is the zero-point energy difference and TΔS is the entropy difference between the gas phase and adsorbed state.

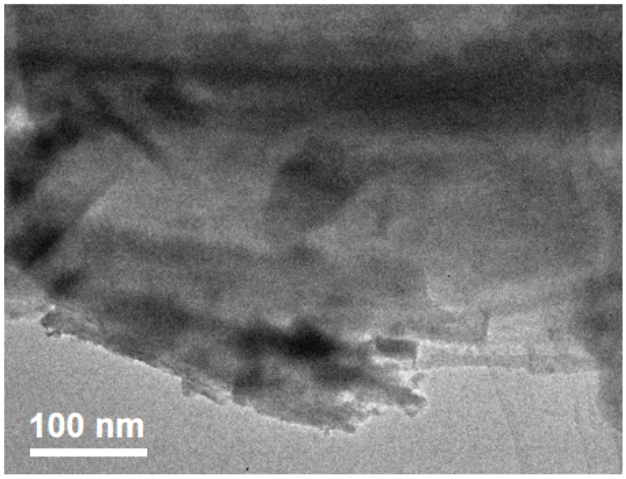

Fig. S1. TEM image of ZnO nanosheets.

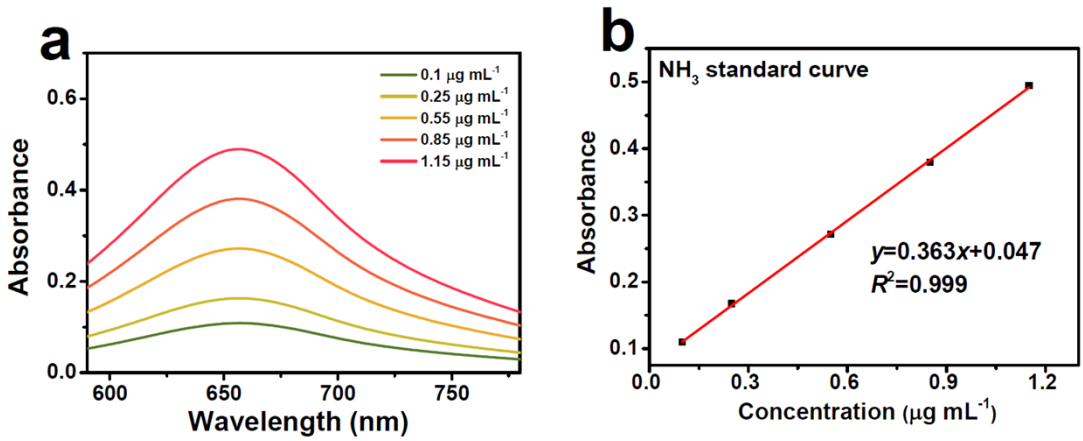

Fig. S2. (a) UV-vis absorption spectra of NH_4^+ assays after incubated for 2 h at ambient conditions. (b) Calibration curve used for the calculation of NH_3 concentrations.

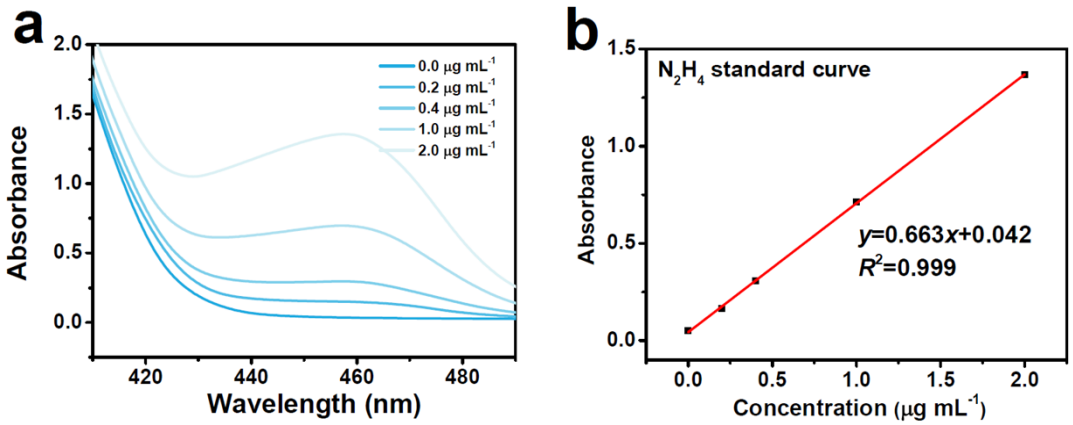

Fig. S3. (a) UV-vis absorption spectra of N_2H_4 assays after incubated for 20 min at ambient conditions. (b) Calibration curve used for calculation of N_2H_4 concentrations.

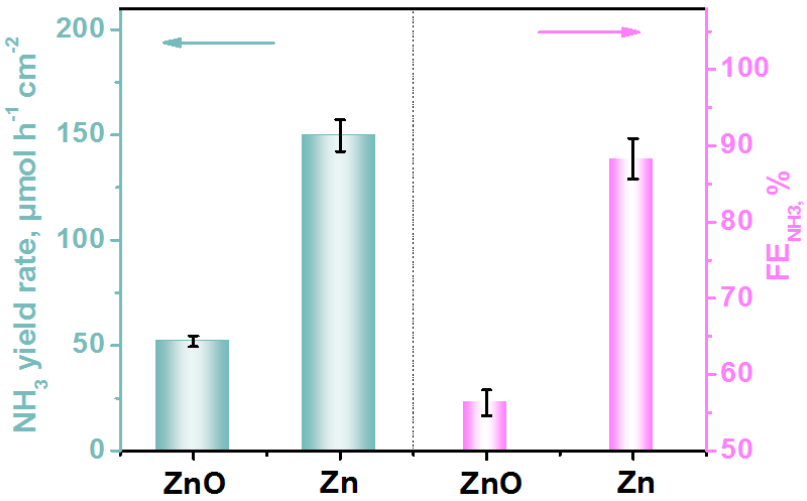

Fig. S4. NH_3 yield rates and FE_{NH3} of ZnO and Zn at -0.8 V.

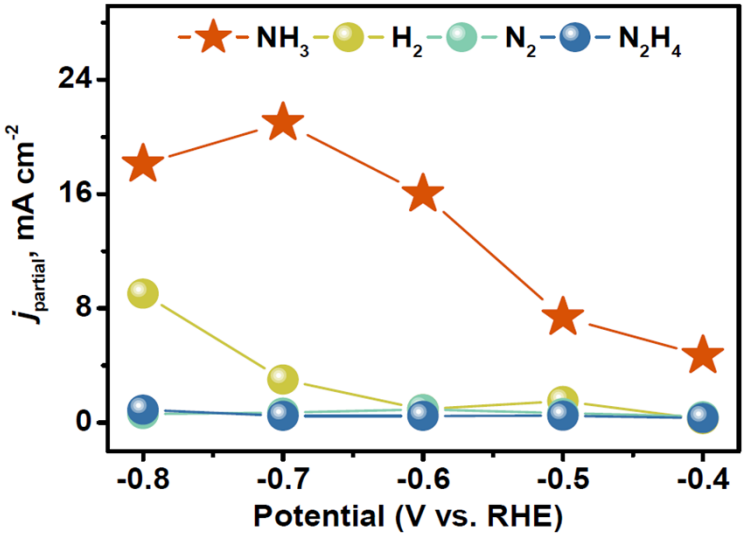

Fig. S5. Partial current densities of various products over Zn nanosheets after 1 h of NORR electrolysis at different potentials.

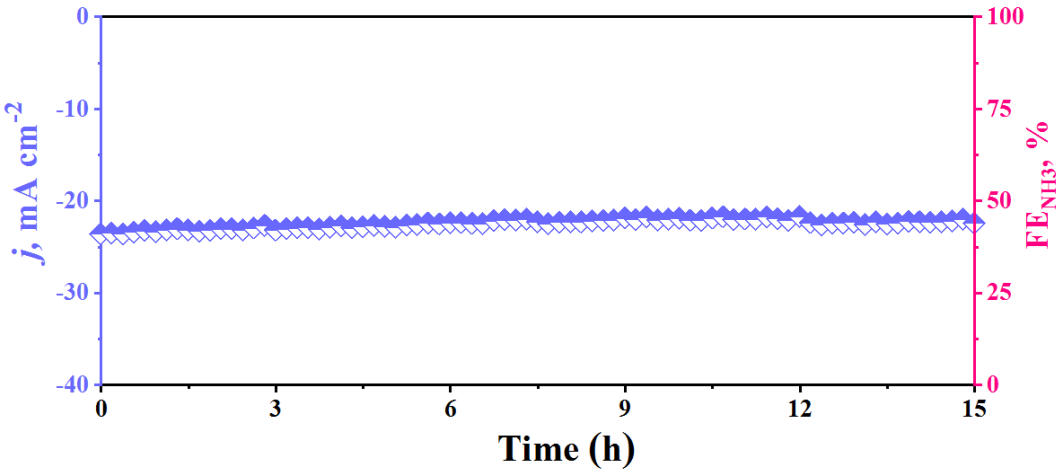

Fig. S6. Chronopotentiometric test of Zn nanosheets for 15 h at -0.8 V.

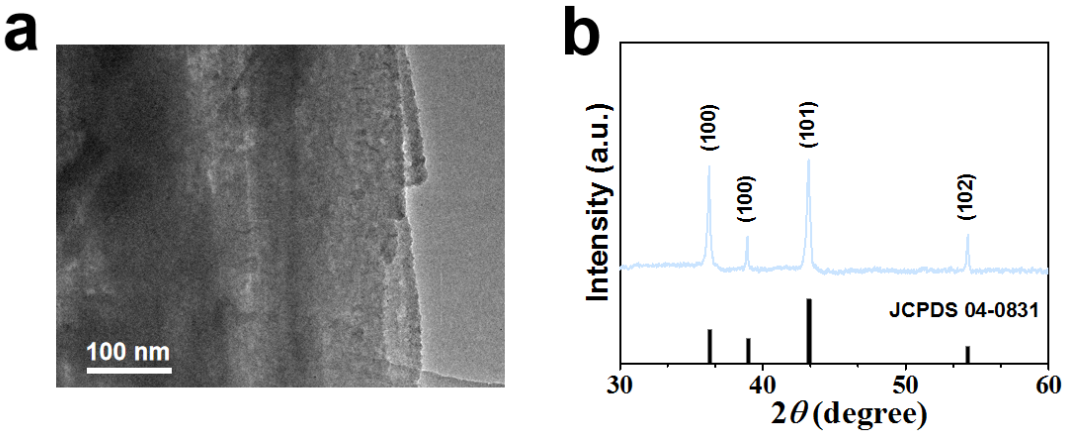

Fig. S7. (a) TEM image and (b) XRD pattern of Zn nanosheets after stability test.

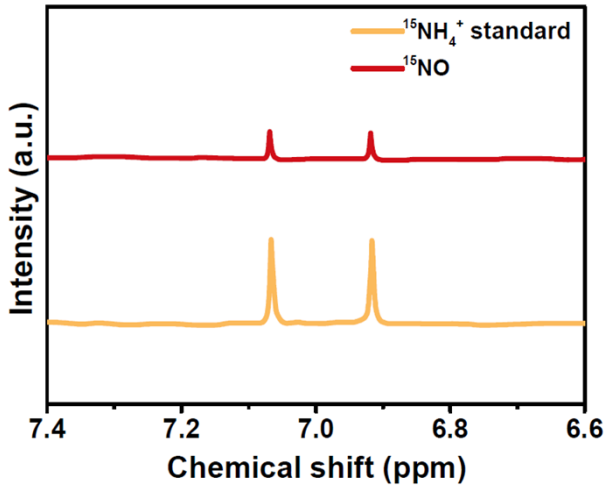

Fig. S8. ^{1}H NMR spectra of $^{15}NH_4^+$ standard sample and those fed by ^{15}NO and Ar after NORR electrolysis on Zn nanosheets at -0.8 V.

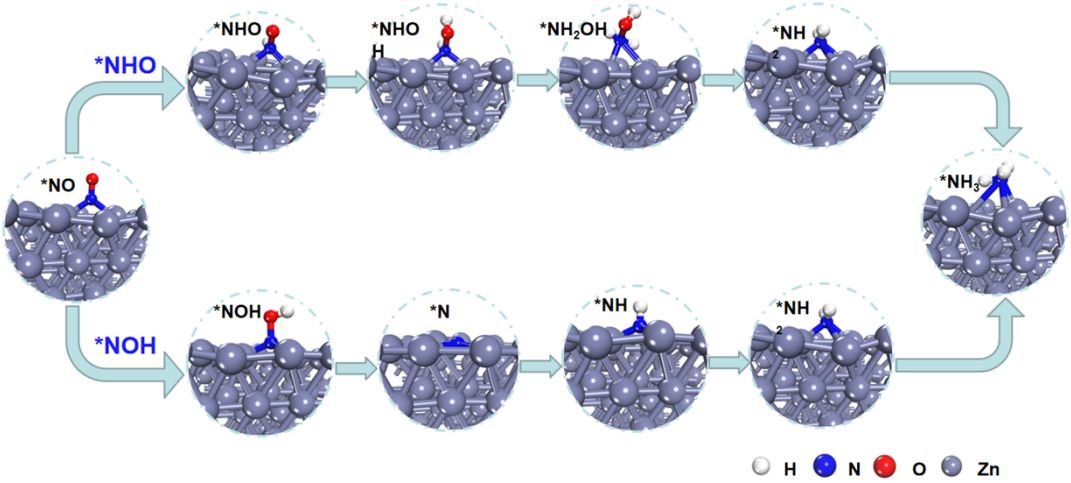

Fig. S9. Schematic of NOH and NHO pathways on on Zn.

Table S1. Comparison of the optimum NH_3 yield rates and NH_3-Faradic efficiency (FE_{NH3}) for recently reported state-of-the-art NORR electrocatalysts at ambient conditions.

Catalyst	Electrolyte	NH_3 yield rate (μmol h^{-1} cm^{-2})	FE_{NH3} (%)	Potential (V vs. RHE)	Ref.
FeP/CC	0.2 M PBS	85.62	88.49	-0.2	[7]
Ni_2P/CP	0.1 M HCl	33.47	76.9	-0.2	[8]
MoS_2/GF	0.1 M HCl	99.6	76.6	0.1	[9]
a-$B_{2.6}C$@TiO_2/Ti	0.1 M Na_2SO_4	216.4	87.6	-0.9	[10]
MnO_{2-x}	0.2 M Na_2SO_4	9.9	82.8	-0.7	[11]
Co_1/MoS_2	0.5 M Na_2SO_4	217.6	87.7	-0.5	[12]
CoP/TM	0.2 M Na_2SO_4	47.22	88.3	-0.2	[13]
Bi/C	0.1 M Na_2SO_4	273.8	93	-0.4	[14]
Bi powder	0.5 M K_2SO_4	2.2	-	-0.65	[15]
Nb_1/BNC	0.1 M HCl	295.2	77.1	-0.6	[16]
Zn nanosheets	**0.5 M Na_2SO_4**	**149.7**	**88.2**	**-0.8**	**This work**

Supplementary references

[1]. Q. Li, J. Wang, Y. Cheng and K. Chu, *J. Energy Chem.*, 2021, **54**, 318-322.

[2]. L. Zhang, J. Liang, Y. Wang, T. Mou, Y. Lin, L. Yue, T. Li, Q. Liu, Y. Luo, N. Li, B. Tang, Y. Liu, S. Gao, A. A. Alshehri, X. Guo, D. Ma and X. Sun, *Angew. Chem. Int. Edit.*, 2021, **60**, 25263-25268.

[3]. Y. Luo, K. Chen, P. Shen, X. Li, X. Li, Y. Li and K. Chu, *J. Colloid Interf. Sci.*, 2023, **629**, 950-957.

[4]. Y. Wang, C. Wang, M. Li, Y. Yu and B. Zhang, *Chem. Soc. Rev.*, 2021, **50**, 6720-6733.

[5]. S. J. Clark, M. D. Segall, C. J. Pickard, P. J. Hasnip, M. I. J. Probert, K. Refson and M. C. Payne, *Z. Kristallogr.*, 2005, **220**, 567-570.

[6]. B. He, P. Lv, D. Wu, X. Li, R. Zhu, K. Chu, D. Ma and Y. Jia, *J. Mater. Chem. A*, 2022, **10**, 18690-18700.

[7]. J. Liang, Q. Zhou, T. Mou, H. Chen, L. Yue, Y. Luo, Q. Liu, M. S. Hamdy, A. A. Alshehri, F. Gong and X. Sun, *Nano Res.*, 2022, **15**, 4008-4013.

[8]. T. Mou, J. Liang, Z. Ma, L. Zhang, Y. Lin, T. Li, Q. Liu, Y. Luo, Y. Liu, S. Gao, H. Zhao, A. M. Asiri, D. Ma and X. Sun, *J. Mater. Chem. A*, 2021, **9**, 24268-24275.

[9]. L. Zhang, J. Liang, Y. Wang, T. Mou, Y. Lin, L. Yue, T. Li, Q. Liu, Y. Luo, N. Li, B. Tang, Y. Liu, S. Gao, A. A. Alshehri, X. Guo, D. Ma and X. Sun, *Angew. Chem. Int. Ed.*, 2021, **133**, 25467-25472.

[10]. J. Liang, P. Liu, Q. Li, T. Li, L. Yue, Y. Luo, Q. Liu, N. Li, B. Tang, A. A. Alshehri, I. Shakir, P. O. Agboola, C. Sun and X. Sun, *Angew. Chem. Int. Ed.*, 2022, **61**, e202202087.

[11]. Z. Li, Z. Ma, J. Liang, Y. Ren, T. Li, S. Xu, Q. Liu, N. Li, B. Tang, Y. Liu, S. Gao, A. A. Alshehri, D. Ma, Y. Luo, Q. Wu and X. Sun, *Mater. Today Phys.*, 2022, **22**, 100586.

[12]. X. Li, K. Chen, X. Lu, D. Ma and K. Chu, *Chem. Eng. J.*, 2023, **454**, 140333.

[13]. J. Liang, W.-F. Hu, B. Song, T. Mou, L. Zhang, Y. Luo, Q. Liu, A. A. Alshehri, M. S. Hamdy, L.-M. Yang and X. Sun, *Inorg. Chem. Front.*, 2022, **9**, 1366-1372.

[14]. Q. Liu, Y. Lin, L. Yue, J. Liang, L. Zhang, T. Li, Y. Luo, M. Liu, J. You, A. A. Alshehri, Q. Kong and X. Sun, *Nano Res.*, 2022, **15**, 5032-5037.

[15]. J. Choi, H.-L. Du, C. K. Nguyen, B. H. R. Suryanto, A. N. Simonov and D. R. MacFarlane, *ACS Energy Lett.*, 2020, **5**, 2095-2097.

[16]. X. Peng, Y. Mi, H. Bao, Y. Liu, D. Qi, Y. Qiu, L. Zhuo, S. Zhao, J. Sun, X. Tang, J. Luo and X. Liu, *Nano Energy*, 2020, **78**, 105321.